International Journal of Power Electronics and Drive System (IJPEDS)
Vol. 7, No. 1, March 2016, pp. 202~216
ISSN: 2088-8694

Critical Condition of Sensorless Induction Generator using Flux Weakening in Wind Turbine Application

Nanda Avianto Wicaksono, Abdul Halim, Aries Subiantoro, Feri Yusivar
Department of Electrical Engineering, University of Indonesia (UI), Indonesia

Article Info

Article history:

Received Oct 10, 2015
Revised Dec 21, 2015
Accepted Jan 11, 2016

Keyword:

Generated power
Rotor speed
Sensorless induction generator
Stability
Wind speed

ABSTRACT

This paper was intended to examine thoroughly a critical condition of the sensorless induction generator using flux weakening in wind turbine application. The critical condition would happen when the rotor speed reached the critical rotor speed reference. The critical rotor speed reference was the highest of the rotor speed reference that still caused the stable response. It was obtained by increasing the rotor speed reference until the system response became unstable. In the low speed range of wind showed that there was no unstable condition whatever a rotor speed reference was set. On the other hand, there was a critical rotor speed reference in the medium and high speed range of wind. The unstable condition was caused by the induction generator that received a power higher than its capacity, so its rotor speed couldn't be maintained at reference value. The first solution was suggested that the stable condition would be made by setting the rotor speed reference at the minimum critical reference. The second solution was suggested that the controlling rotor speed in triangle area between the critical condition and the operation that used the minimum critical reference for the rotor speed reference. In the triangle area, the rotor speed was controlled by setting the tip speed ratio.

Corresponding Author:

Nanda Avianto Wicaksono,
Department of Electrical Engineering,
University of Indonesia,
Kampus UI Depok, Jakarta, 16424 Indonesia.
Email: nandaavianto@gmail.com

1. INTRODUCTION

There was a potency of wind energy in many locations which were far from cities, areas with the small and low density of population, and were having small economic activities. The locations fitted to be developed by using small wind turbines. The small wind turbines should have low cost, high reliability and low maintenance.

For efficient cost and simple purpose application, the small wind turbine was designed by using (a) a sensorless squirrel cage induction generator (SCIG), (b) fixed pitch angle of blades, and (c) fixed gear ratio. This configuration of the wind turbine was chosen because of its simple construction, simple maintenance, reliable operation, and also low price.

The fixed pitch angle of blades caused that the wind turbine couldn't limit a received power from wind. The received power that was higher than the rated power caused the generator became over-voltages and over-current. To protect the generator damage caused of the over-voltages and the over-current, the wind turbine operation must be stopped when a wind speed became higher than its rated speed. The stopping caused the generated power couldn't be produced.

To make the wind turbine able to generate power in a high speed of wind, the system was equipped by a flux weakening control algorithm. The flux weakening control would keep the voltages and currents

generator ranged within the rated values. In [1], Yusivar *et al.* had simulated the wind turbine induction generator using flux weakening. The simulation showed the unstable condition at the over-speed operation. To define the variable which caused the unstable condition, the Yusivar et al.'s research should be continued by analyzing a boundary between the stable and the unstable conditions. The boundary between the stable and the unstable conditions was called the critical condition.

The main contribution of this paper was to examine thoroughly the critical condition of the sensorless induction generator using flux weakening in wind turbine application and define the variable which caused the unstable condition.

2. RESEARCH METHOD

This research consisted of four stages, i.e. (1) mathematical modelling, (2) implementation, (3) simulation, and (4) analysis.

2.1. The Mathematical Modelling

The model of the system consisted of three parts, i.e. (1) the mechanical of wind turbine, (2) the induction generator, and (3) the controller (see Figure 1).

First, the mechanical of wind turbine was used for calculating a load torque that referred to the rotor speed of induction generator and the wind speed.

Second, the model of induction generator was used to produce the stator currents that refer to stator voltages and a load torque. The stator voltages were the output of the controller, while the load torque was received from the mechanical of wind turbine.

Third, the controller consisted of (1) a three phases to two phases transform and vice versa, (2) a pulse width modulation (PWM) generator, (3) a rotor flux orientation control (RFOC), (4) a flux weakening, (5) a speed controller, and also (6) an observer to estimate the rotor speed. The block diagram of the controller was shown in Figure 2.

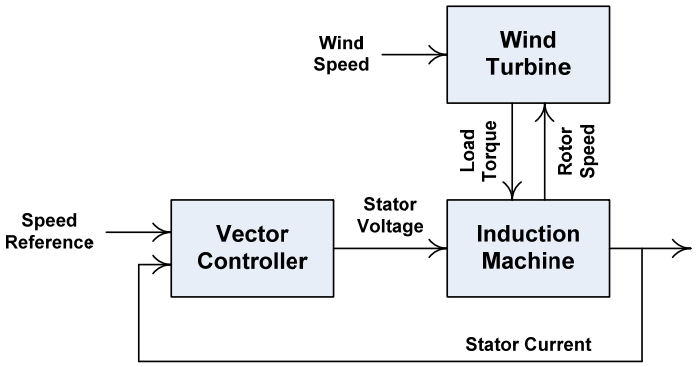

Figure 1. The parts of system

This research used the wind turbine type of horizontal axis. Its blades were connected to the low speed shaft that wasn't directly connected to the induction generator. There was a gearbox between the low speed shaft and the induction generator. The gearbox was used to increase the speed of the low speed shaft.

The model of the mechanical wind turbine used six equations (1-6). The equations was used to calculate the capacity factor of the wind turbine (C_p), the turbine speed (ω_{wt}), the tip speed ratio (λ), the turbine power (P_{wt}), and the load torque (T_L) [2], [3].

$$C_p(\lambda, i) = 0.22\left(\frac{116}{\lambda_i} - 0.4i - 5\right)\exp\left(\frac{-12.5}{\lambda_i}\right) \quad (1)$$

$$\omega_{wt} = \frac{\omega_r}{K_G} \quad (2)$$

$$\lambda = \frac{r\,\omega_{wt}}{V} \quad (3)$$

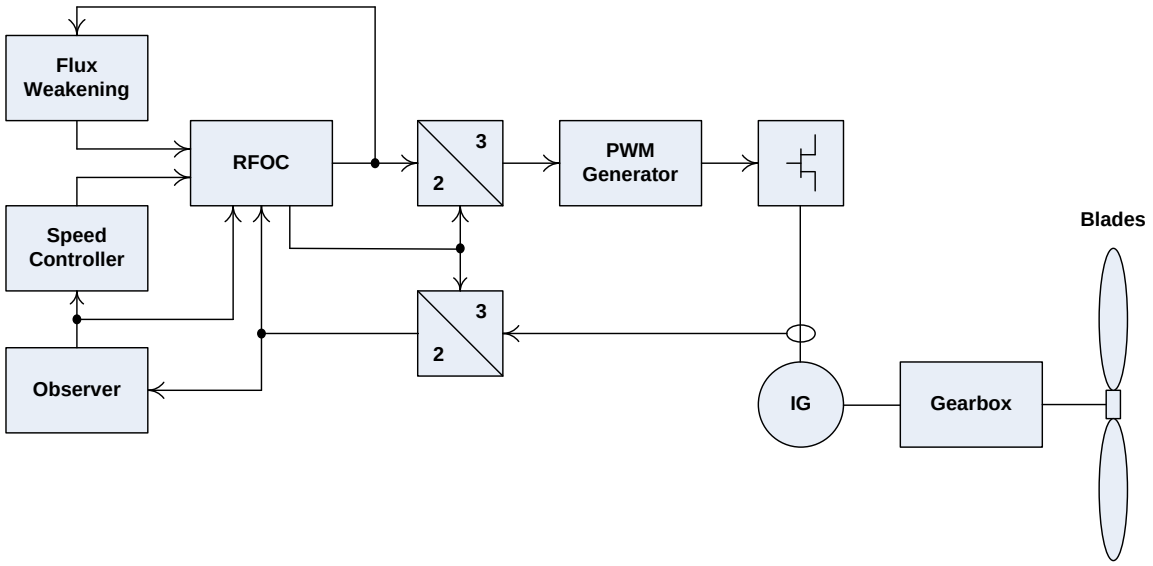

Figure 2. Block diagram of the controller

$$\frac{1}{\lambda_i} = \frac{1}{\lambda + 0.08i} - \frac{0.035}{i^3 + 1} \tag{4}$$

$$P_{wt} = 0.5\,\rho\,\pi\,R^2\,V^3\,C_p \tag{5}$$

$$T_L = \frac{P_{wt}}{\omega_r} \tag{6}$$

The model of the induction generator used seven differential equations, i.e. the differential equation of the stator current in d-axis (i_{sd}) (7), the differential equation of the stator current in q-axis (i_{sq}) (8), the differential equation of the rotor current in d-axis (i_{rd}) (9), the differential equation of the rotor current in q-axis (i_{rq}) (10), the differential equation of the angular speed of the stator voltage (θ_e) (11), the differential equation of the rotor speed (ω_r) (12), and the differential equation of the angle of rotor (13) [4], [5].

$$\frac{d}{dt} i_{sd} = \frac{1}{\sigma L_s} v_{sd} - \left(\frac{R_s}{\sigma L_s} + \frac{(1-\sigma)}{\sigma \tau_r}\right) i_{sd} + \frac{(1-\sigma)}{\sigma \tau_r} i_{rd} + \frac{(1-\sigma) N_p \omega_r}{\sigma} i_{rq} + \omega_e i_{sq} \tag{7}$$

$$\frac{d}{dt} i_{sq} = \frac{1}{\sigma L_s} v_{sq} - \left(\frac{R_s}{\sigma L_s} + \frac{(1-\sigma)}{\sigma \tau_r}\right) i_{sq} + \frac{(1-\sigma)}{\sigma \tau_r} i_{rq} - \frac{(1-\sigma) N_p \omega_r}{\sigma} i_{rd} - \omega_e i_{sd} \tag{8}$$

$$\frac{d}{dt} i_{rd} = -\frac{R_r}{L_r} i_{rd} + \frac{R_r}{L_r} i_{sd} + \left(\omega_e - N_p \omega_r\right) i_{rq} \tag{9}$$

$$\frac{d}{dt} i_{rq} = -\frac{R_r}{L_r} i_{rq} + \frac{R_r}{L_r} i_{sq} - \left(\omega_e - N_p \omega_r\right) i_{rd} \tag{10}$$

$$\frac{d}{dt} \theta_e = N_p \omega_r + \frac{i_{sq}}{\tau_r i_{mr}} \tag{11}$$

$$\frac{d}{dt} \omega_r = \frac{1}{J} (T_e - T_L - B.\omega_r) \tag{12}$$

$$\frac{d}{dt} \theta_r = \omega_r \tag{13}$$

Before using the differential equations, the stator voltages received from the PWM generator were converted by the three phases (abc) to two phases (dq-axis) transformation. And after using the differential equations, the rotor currents produced were converted by the two phases (dq-axis) to three phases (abc) transformation.

To convert the stator voltage from the three phases (abc-axis) to the two phases (dq-axis) was used the Clarke transform (14) and then the Park transform (15). Viceversa, to convert the stator current from the two phases (dq-axis) to the three phases (abc-axis) was used the Park inverse transform (16) and then the Clarke inverse transform (17). The converting voltages or currents from the three phases (abc-axis) to the two phases (dq-axis) and viceversa were also used in the controller [6], [7].

$$\begin{bmatrix} v_{s\alpha} \\ v_{s\beta} \end{bmatrix} = \sqrt{\frac{2}{3}} \begin{bmatrix} 1 & -0.5 & -0.5 \\ 0 & 0.5\sqrt{3} & -0.5\sqrt{3} \end{bmatrix} \begin{bmatrix} v_{sa} \\ v_{sb} \\ v_{sc} \end{bmatrix} \quad (14)$$

$$\begin{bmatrix} v_{sd} \\ v_{sq} \end{bmatrix} = \begin{bmatrix} \cos\theta_e & \sin\theta_e \\ -\sin\theta_e & \cos\theta_e \end{bmatrix} \begin{bmatrix} v_{s\alpha} \\ v_{s\beta} \end{bmatrix} \quad (15)$$

$$\begin{bmatrix} i_{s\alpha} \\ i_{s\beta} \end{bmatrix} = \begin{bmatrix} \cos\theta_e & -\sin\theta_e \\ \sin\theta_e & \cos\theta_e \end{bmatrix} \begin{bmatrix} i_{sd} \\ i_{sq} \end{bmatrix} \quad (16)$$

$$\begin{bmatrix} i_{sa} \\ i_{sb} \\ i_{sc} \end{bmatrix} = \sqrt{\frac{2}{3}} \begin{bmatrix} 1 & 0 \\ -0.5 & 0.5\sqrt{3} \\ -0.5 & 0.5\sqrt{3} \end{bmatrix} \begin{bmatrix} i_{s\alpha} \\ i_{s\beta} \end{bmatrix} \quad (17)$$

The PWM generator was comparing the absolute value of the stator voltage references with the triangle carrier. If the absolute value was higher than the triangle carrier, the switch was on. Vice versa, if the absolute value was lower than the triangle carrier, the switch was off.

While the switch was on and the stator voltage reference was positive, the stator voltage of the induction generator was the same as the PWM amplitude of +Vdc/2. Vice versa, the stator voltage of the induction generator was -Vdc/2 while the switch was on and the stator voltage reference was negative (see Figure 3) [8].

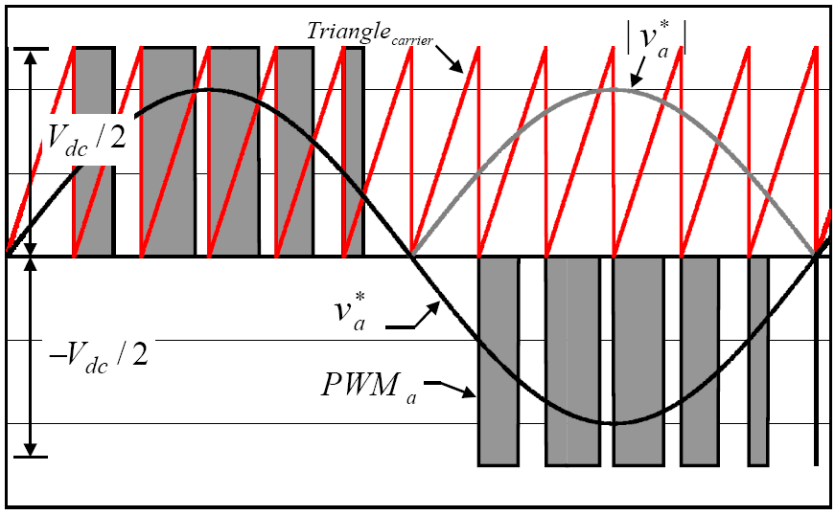

Figure 3. Generating PWM signal

The stator voltage references (v_{sd} and v_{sq}) that were received by the PWM generator contained the linier references (u_{sdlin} and u_{sqlin}) and the nonlinier decoupling references (u_{sddec} and u_{sqdec}). The linier references was adjusted from two PI controllers. The adjusting PI controllers referred to the error between the

rotor current references and the actual values. On the other hand, the nonlinier decoupling references were calculated by equations (22) and (23) [8].

$$v_{sd} = u_{sdlin} + u_{sddec} \tag{18}$$

$$v_{sq} = u_{sqlin} + u_{sqdec} \tag{19}$$

$$u_{sdlin} = K_{pid}\left(i_{sdref} - i_{sd}\right) + K_{iid}\int\left(i_{sdref} - i_{sd}\right)dt \tag{20}$$

$$u_{sqlin} = K_{piq}\left(i_{sqref} - i_{sq}\right) + K_{iiq}\int\left(i_{sqref} - i_{sq}\right)dt \tag{21}$$

$$u_{sddec} = -\omega_e L_s \sigma i_{sq} + L_s(1-\sigma)\frac{d}{dt}i_{mr} \tag{22}$$

$$u_{sqdec} = \omega_e L_s \sigma i_{sd} + L_s(1-\sigma)\omega_e i_{mr} \tag{23}$$

The equations (20) and (21) showed that the calculating linier references used the stator current references (i_{sdref} and i_{sqref}) from the flux weakening. The flux weakening limited the stator current references of the induction generator by using equations (24-28). The flux weakening received the stator current reference in q-axis (i_{sqref}) from the speed controller of PI controller. The adjusting PI controller referred to the error between the rotor speed reference (ω_{rref}) and the actual rotor speed (ω_r) (see equation (29)) [9], [10].

$$e_{v2} = {v_{smax}}^2 - ({v_{sd}}^2 + {v_{sq}}^2) \tag{24}$$

$$i_{sdref} = K_{pimr}e_{v2} + K_{iimr}\int e_{v2}dt \tag{25}$$

$$i_{sdref} \leq i_{imrmax} \tag{26}$$

$$i_{isqmax} = \sqrt{{i_{smax}}^2 - {i_{sdref}}^2} \tag{27}$$

$$\left|i_{sqref}\right| \leq \left|i_{isqmax}\right| \tag{28}$$

$$i_{sqref} = K_{p\omega}\left(\omega_{rref} - \omega_r\right) + K_{i\omega}\int\left(\omega_{rref} - \omega_r\right)dt \tag{29}$$

The equations (22) and (23) showed that the calculating nonlinier decoupling references needed the stator speed (ω_e) and the rotor magnetizing current (i_{mr}) form RFOC. Besides the stator speed and the rotor magnetizing current, RFOC also calculated the electric torque of the induction generator (T_e) and the stator angle (θ_e) [8].

$$\omega_e = N_p\omega_r + \frac{1}{\tau_r}\frac{i_{sq}}{i_{mr}} \tag{30}$$

$$T_e = N_p(1-\sigma)L_s i_{sq} i_{mr} \tag{31}$$

$$\frac{d}{dt}\theta_e = \omega_e \tag{32}$$

$$\frac{d}{dt}i_{mr} = \frac{1}{\tau_r}i_{sq} - \frac{1}{\tau_r}i_{mr} \tag{33}$$

The equation (29) showed that the speed controller needed the actual rotor speed (ω_r) from the induction motor. But the actual rotor speed couldn't be obtained form the sensorless induction generator. The feed back signals form the the sensorless induction generator were mainly the stator currents.

To subtitute the actual rotor speed (ω_r), the controller was equipped with an observer. The observer was used to estimate the rotor speed by using equation (34). The estimated rotor speed was calculated by using the estimated rotor flux (ψ_{rdest} and ψ_{rqest}) and the *error* (e_{isd} and e_{isq}) between the estimated stator currents and the actual values [11].

$$\omega_{rest} = K_p\left(\psi_{rqest}\, e_{isd} - \psi_{rdest}\, e_{isq}\right) + K_i \int \left(\psi_{rqest}\, e_{isd} - \psi_{rdest}\, e_{isq}\right)dt \tag{34}$$

$$i_{sqref} = K_{p\omega}\left(\omega_{rref} - \omega_{rest}\right) + K_{i\omega} \int \left(\omega_{rref} - \omega_{rest}\right)dt \tag{35}$$

In this research, the estimation of the rotor magnetizing fluxes and the stator currents used the Luenberger observer. The Luenberger observer was able to estimate the state variables (***X***) and the output variables (***Y***) in the state space (36) and (37) [11]. The estimated state variables ($\boldsymbol{X_{est}}$) and the estimated output variables ($\boldsymbol{Y_{est}}$) could be calculated by using equations (37) and (38) [12], [13].

$$\frac{d}{dt}X = AX + BU \tag{36}$$

$$Y = CX \tag{37}$$

$$\frac{d}{dt}X_{est} = AX_{est} + BU + G(Y - Y_{est}) \tag{38}$$

$$Y_{est} = CX_{est} \tag{39}$$

By using the equations (38) and (39), the Luenberger observer in the equation (41) was used to estimate the state variables of the induction generator (i_{sd}, i_{sq}, Ψ_{rd}, and Ψ_{rq}) in the equation (40). The estimated state variables were i_{sdest}, i_{sqest}, Ψ_{rdest}, and Ψ_{rqest} [11], [12], [13].

$$\frac{d}{dt}\begin{bmatrix} i_{sd} \\ i_{sq} \\ \psi_{rd} \\ \psi_{rq} \end{bmatrix} = \begin{bmatrix} -\left(\frac{R_s}{\sigma L_s} + \frac{(1-\sigma)}{\sigma\tau_r}\right) & \omega_e & \frac{L_m}{\sigma L_s L_r \tau_r} & \frac{L_m N_p \omega_r}{\sigma L_s L_r} \\ -\omega_e & \frac{1}{\sigma L_s}\left(-R_s - \frac{{L_m}^2}{\tau_r L_r}\right) & -\frac{L_m N_p \omega_r}{\sigma L_s L_r} & \frac{L_m}{\sigma L_s \tau_r L_r} \\ \frac{R_r}{L_r}L_m & 0 & -\frac{1}{\tau_r} & (\omega_e - N_p\omega_r) \\ 0 & \frac{L_m}{\tau_r} & -(\omega_e - N_p\omega_r) & \frac{1}{\tau_r} \end{bmatrix} \begin{bmatrix} i_{sd} \\ i_{sq} \\ \psi_{rd} \\ \psi_{rq} \end{bmatrix} + \begin{bmatrix} \frac{1}{\sigma L_s} & 0 \\ 0 & \frac{1}{\sigma L_s} \\ 0 & 0 \\ 0 & 0 \end{bmatrix} \begin{bmatrix} v_{sd} \\ v_{sq} \end{bmatrix} \tag{40}$$

$$\begin{bmatrix} i_{sd} \\ i_{sq} \\ \psi_{rd} \\ \psi_{rq} \end{bmatrix} = \begin{bmatrix} 1 & 0 & 0 & 0 \\ 0 & 1 & 0 & 0 \\ 0 & 0 & 1 & 0 \\ 0 & 0 & 0 & 1 \end{bmatrix} \begin{bmatrix} i_{sd} \\ i_{sq} \\ \psi_{rd} \\ \psi_{rq} \end{bmatrix}$$

$$\frac{d}{dt}\begin{bmatrix} i_{sdest} \\ i_{sqest} \\ \psi_{rdest} \\ \psi_{rqest} \end{bmatrix} = \begin{bmatrix} -\left(\frac{R_s}{\sigma L_s}+\frac{(1-\sigma)}{\sigma\tau_r}\right) & \omega_e & \frac{L_m}{\sigma L_s L_r \tau_r} & \frac{L_m N_p \omega_r}{\sigma L_s L_r} \\ -\omega_e & \frac{1}{\sigma L_s}\left(-R_s-\frac{{L_m}^2}{\tau_r L_r}\right) & -\frac{L_m N_p \omega_r}{\sigma L_s L_r} & \frac{L_m}{\sigma L_s \tau_r L_r} \\ \frac{R_r}{L_r}L_m & 0 & -\frac{1}{\tau_r} & (\omega_e - N_p\omega_r) \\ 0 & \frac{L_m}{\tau_r} & -(\omega_e - N_p\omega_r) & \frac{1}{\tau_r} \end{bmatrix} \begin{bmatrix} i_{sdest} \\ i_{sqest} \\ \psi_{rdest} \\ \psi_{rqest} \end{bmatrix} \quad (41)$$

$$+\begin{bmatrix} \frac{1}{\sigma L_s} & 0 \\ 0 & \frac{1}{\sigma L_s} \\ 0 & 0 \\ 0 & 0 \end{bmatrix}\begin{bmatrix} v_{sd} \\ v_{sq} \end{bmatrix} + \begin{bmatrix} g_1 & -g2 \\ g_2 & g_1 \\ g_3 & -g_4 \\ g_4 & g_3 \end{bmatrix}\begin{bmatrix} i_{sd}-i_{sdest} \\ i_{sq}-i_{isqest} \end{bmatrix}$$

$$\begin{bmatrix} i_{sdest} \\ i_{sqest} \\ \psi_{rdest} \\ \psi_{rqest} \end{bmatrix} = \begin{bmatrix} 1 & 0 & 0 & 0 \\ 0 & 1 & 0 & 0 \\ 0 & 0 & 1 & 0 \\ 0 & 0 & 0 & 1 \end{bmatrix}\begin{bmatrix} i_{sdest} \\ i_{sqest} \\ \psi_{rdest} \\ \psi_{rqest} \end{bmatrix}$$

The equation (41) used the gains g_1, g_2, g_3, and g_4 that were written as below:

$$g_1 = \frac{(k-1)}{k}\left(-\frac{R_s}{\sigma L_s}-\frac{R_r}{\sigma L_r}\right) \quad (42)$$

$$g_2 = -\frac{(k-1)}{k}N_p\omega_r \quad (43)$$

$$g_3 = \frac{(k-1)}{k({\tau_r}^2{N_p}^2{\omega_{rest}}^2+1)}\left(\frac{R_s R_r \tau_r + L_s R_r - \sigma\tau_r L_s L_r {N_p}^2{\omega_{rest}}^2}{L_m}\right) \quad (44)$$

$$g_4 = \frac{(k-1)}{k({\tau_r}^2{N_p}^2{\omega_{rest}}^2+1)}\left(\frac{(R_s L_r \tau_r + R_r L_s \tau_r - \sigma L_s L_r)N_p\omega_{rest}}{L_m}\right) \quad (45)$$

2.2. Implementation

The mathematics model of wind turbine system was written in the C MEX S-Functions and simulated by using MATLAB/SIMULINK. The realization of wind turbine model was shown in Figure 4. The induction generator was a squirrel cage induction machine with the rated power of 1 hp power, the rated speed of 140 rad/s, and the maximum torque of 5 Nm. The parameters of the wind turbine and the induction generator were listed in Table 1.

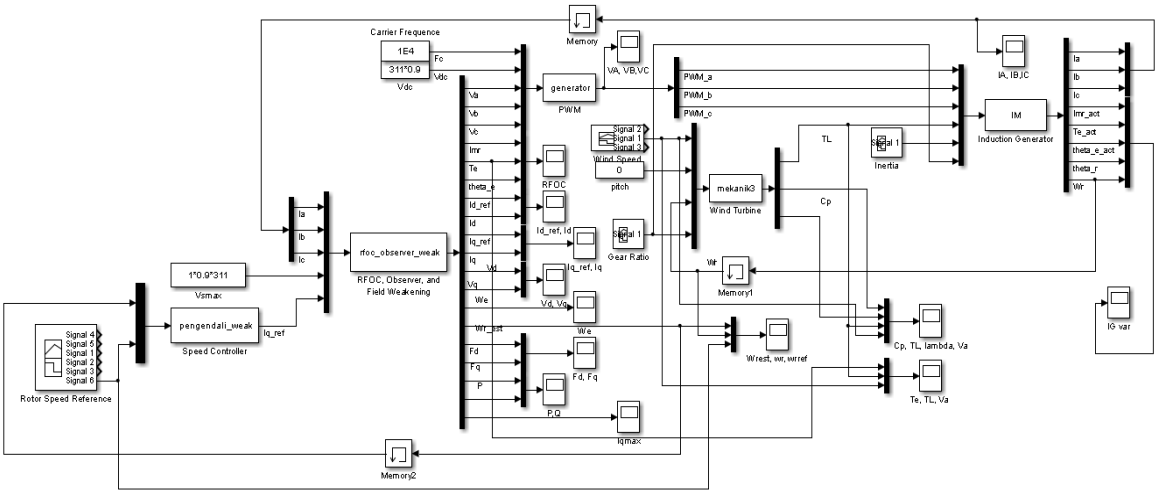

Figure 4. The realization of wind turbine model

Table 1. Wind turbine and induction generator parameters

Symbols	Description	Value	Units
R	Blades Radius	0.95	m
K_G	*Gearbox ratio*	6.65	-
Np	Number of Pole Pairs	2	-
L_s	Stator Inductance	234.9	mH
Lr	Rotor Inductance	234.9	mH
L_m	Mutual Inductance	227.9	mH
R_s	Stator Resistance	2.75	Ω
R_r	Rotor Resistance	2.9	Ω

2.3. Test Scenario

The testing of the system was done by giving a constant wind speed and a constant rotor speed reference. There were two series of wind speed that were tested. The first series, the wind speeds were between 3 m/s and 20 m/s with interval of 1 m/s. The second series, the wind speeds were between 25 m/s and 45 m/s with interval of 5 m/s. For each wind speed, the incremental of rotor speed reference was applied until the system response became unstable. The highest of the rotor speed reference that caused the stable response was named the critical rotor speed reference.

3. RESULTS AND ANALYSIS

3.1. The System Stability

The simulation showed that there were two operating condition responses, i.e. (a) the unstable condition response and (b) the stable condition response. The example of the unstable response was at the rotor speed reference of 240 rad/s and wind speed changed from 6 m/s to 12 m/s (see Figure 5). On the other hand, the example of stable response was at the rotor speed reference of 270 rad/s and wind speed changed from 22 m/s to 30 m/s (see Figure 6). Both condition showed that the system stability didn't only depend on either the rotor speed reference or the wind speed.

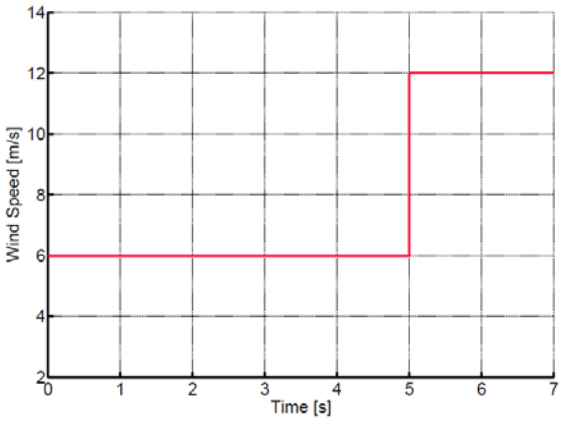

(a) Wind speed changed from 6 m/s to 12 m/s

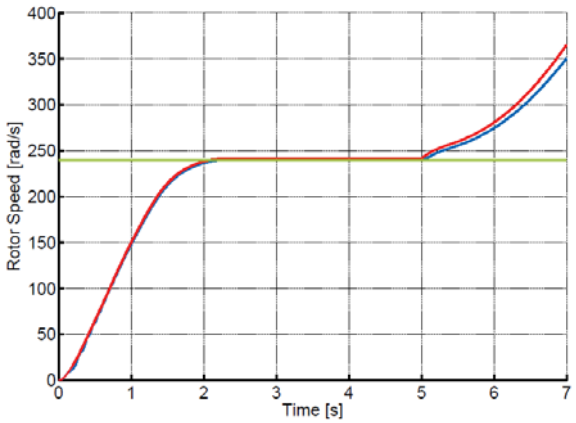

(b) Rotor speed: the reference (green), the actual (red), and the estimated (blue)

Figure 5. The unstable response at the rotor speed reference of 240 rad/s and the wind speed changed from 6 m/s to 12 m/s

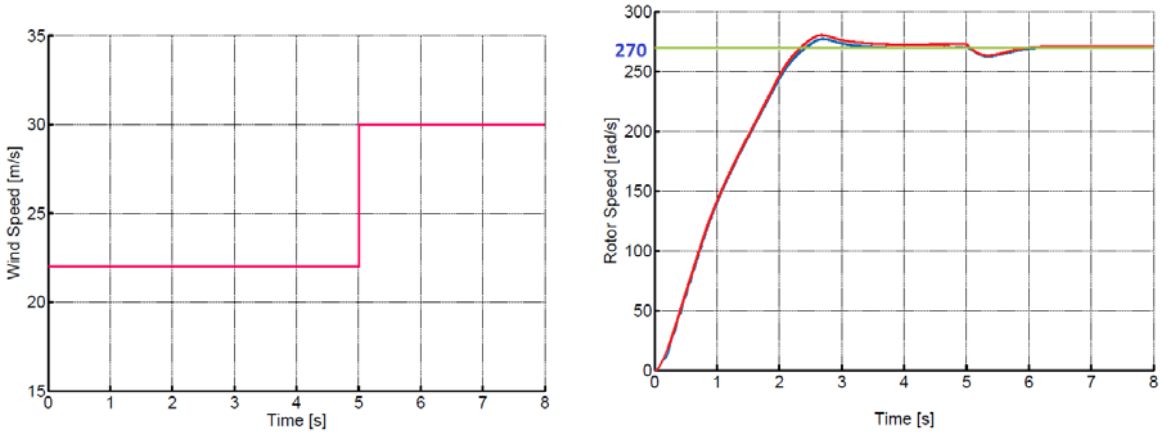

(a) Wind speed changed from 22 m/s to 30 m/s

(b) Rotor speed: the reference (green), the actual (red), and the estimated (blue)

Figure 6. The stable response at the rotor speed reference of 270 rad/s and the wind speed changed from 22 m/s to 30 m/s

3.2. Analysis

The test resulted that there were two operating ranges. First, the low speed range of wind was at the wind speed lower than 8 m/s. Second, the medium and high speed ranges of wind were at the wind speed equal or higher than 8 m/s.

In the low speed range of wind, there wasn't unstable condition whatever a rotor speed reference was set. The highest generated power was reached by the highest capacity factor of 43.8% (see Figure 7). The highest capacity factor was named the optimum operation condition. The highest capacity factor was reached by the optimum tip speed ratio of 6.35 (see Figure 8). At the optimum condition, the generated power was still lower than the power capacity of the induction generator.

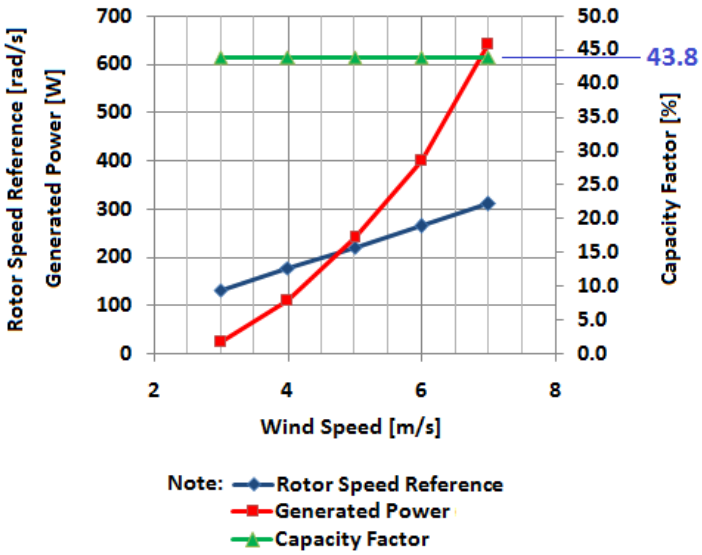

Figure 7. The optimal condition in the low speed range of wind

In Figure 8, the optimum operation condition was shown by point M. At the constant wind speed, the increasing rotor speed reference caused the increasing tip speed ratio, then it would cause decreasing capacity factor (see arrow a in Figure 8). On the other hand, the decreasing rotor speed reference caused a decreasing tip speed ratio, and then it would cause a decreasing capacity factor too (see arrow b in Figure 8).

Both decreasing capacity factor made the lower generated power. Therefore, the rotor speed reference that was higher or lower than the optimum reference would decrease the generated power, so the generated power never exceeded the power capacity of the induction generator.

In the medium and high speed range of wind, there was a critical rotor speed reference. A rotor speed reference that was higher than the critical reference would cause unstable condition. The critical condition occurred while the rotor speed reference was between 230 and 406 rad/s, the load torque of the induction generator was between -2.5 and -5.2 Nm., the generated power was between 725 and 880 W., and the capacity factor was between 0.19 and 42.44 % (see Figure 9). These showed that the load torque and the capacity factor of the critical condition were depending on the rotor speed reference. On the other hand, the generated power of the critical condition was a relative constant around the rated power of 1 hp or 746 W (see Figure 9c). It showed that unstable condition was caused by the induction generator that received a power higher than its capacity, so its rotor speed couldn't be maintained at reference value.

In Figure 8, the critical condition was shown by points in C range. The increasing rotor speed reference caused increasing tip speed ratio and then it would cause increasing capacity factor (see arrow d in Figure 8). The increasing capacity factor caused the increasing generated power then it made the generated power was higher than the rating power motor, so the system would be unstable.

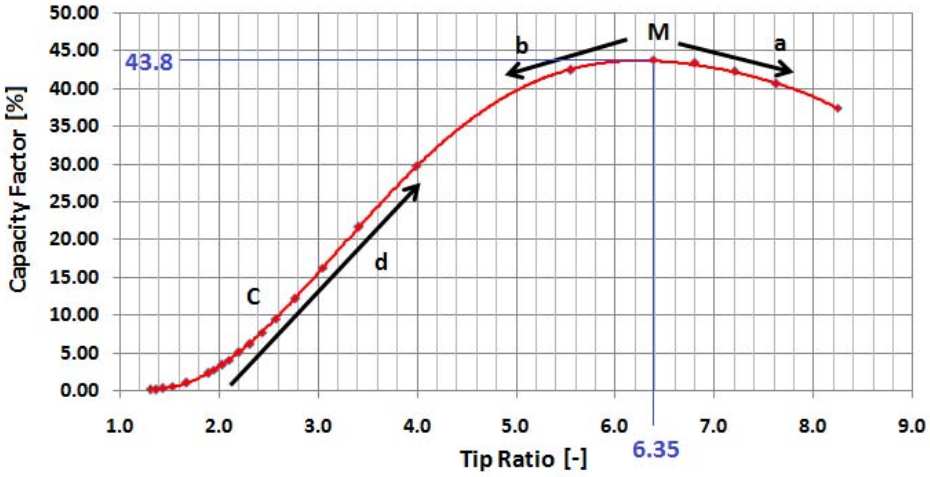

Figure 8. Relation between capacity factor and tip speed ratio

The simulation shown in Figure 5 could be described by two points A and B. Point A represented the condition at the rotor speed reference of 240 rad/s and the wind speed 6 m/s. Point B represented the condition at the rotor speed reference of 240 rad/s and wind speed 12 m/s. The stable condition at point A changed into the unstable condition at point B (see arrow AB in Figure 9a).

On the other hand, the simulation shown in Figure 6 could be described by two points C and D. Point C represented the condition at the rotor speed reference of 270 rad/s and the wind speed 22 m/s. Point D represented the condition at the rotor speed reference of 270 rad/s and wind speed 30 m/s. Both conditions at point C and D were stable (see arrow CD in Figure 9a).

Figure 9 also showed the minimum critical rotor speed reference that was 230 rad/s at the wind speed of 12 m/s. A solution was suggested that the stable condition would be made by setting the rotor speed reference at the minimum critical reference of 230 rad/s. If the rotor speed reference was set constantly at 230 rad/s, the generated power never exceeded the power capacity of the induction generator (see Figure 10). The simulation showed that the system response was stable at the constant rotor speed reference of 230 rad/s although wind speed changed in range 6-45 m/s (see Figure 11).

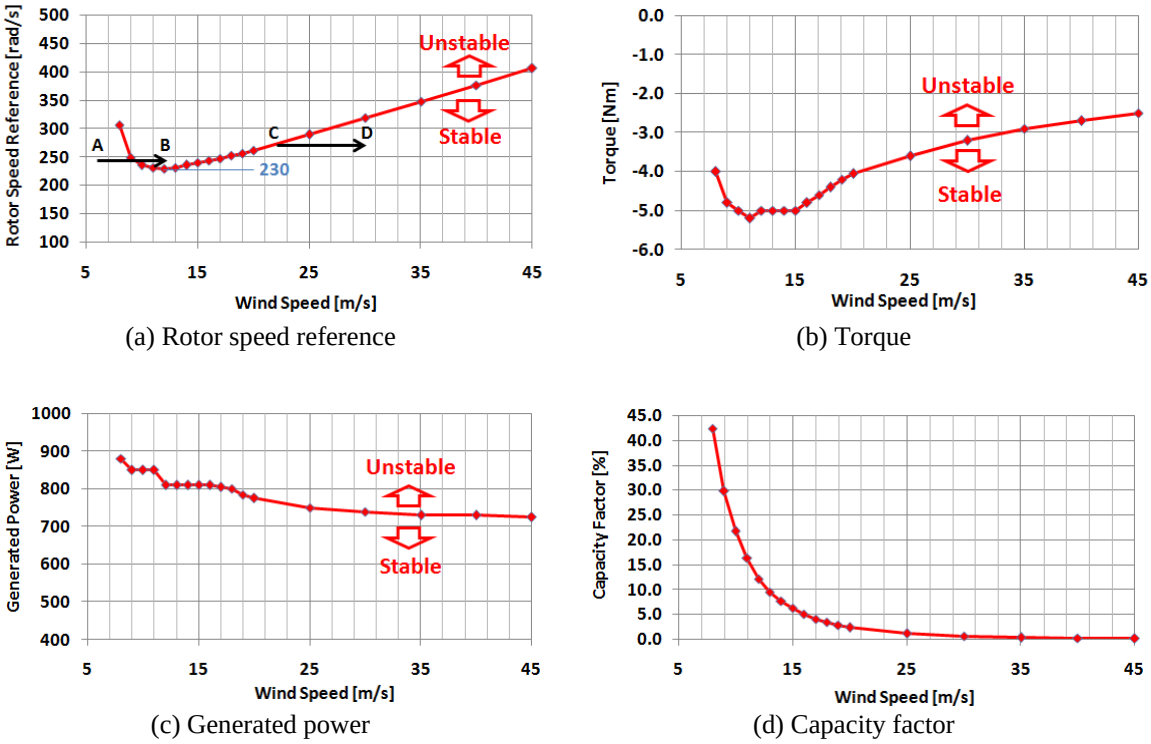

(a) Rotor speed reference (b) Torque

(c) Generated power (d) Capacity factor

Figure 9. The critical condition in the medium and high speed ranges of wind.

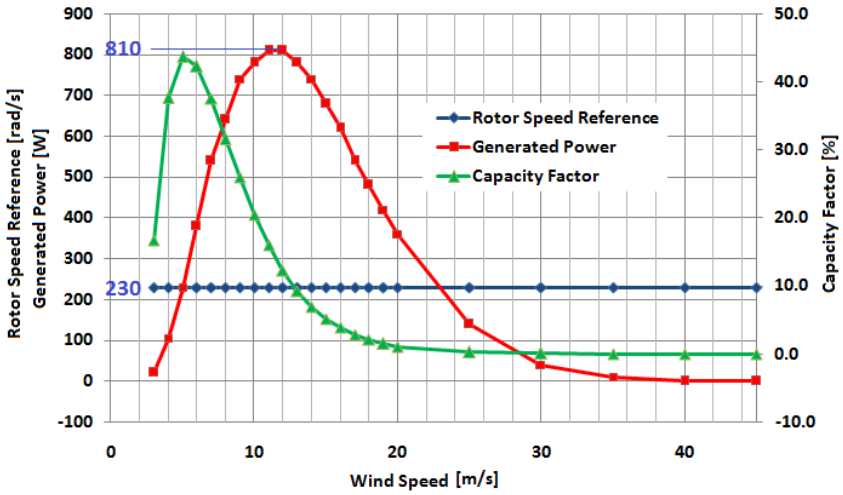

Figure 10. The generated power and the capacity factor with the constant rotor speed reference at 230 rad/s

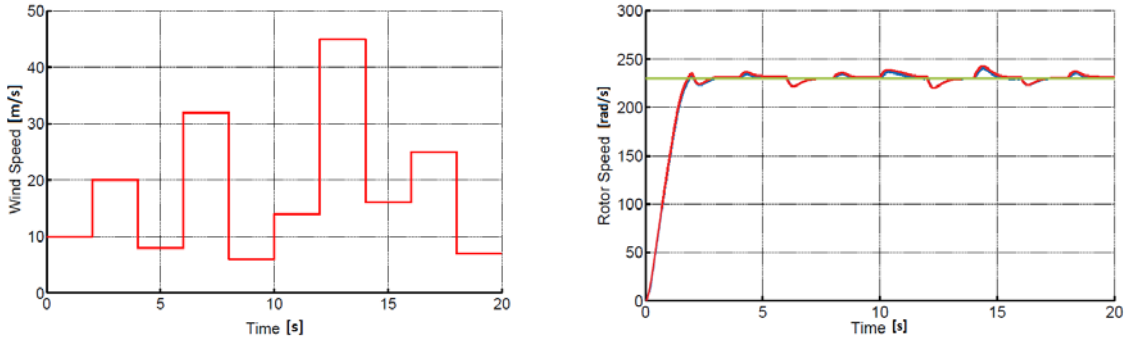

(a) Wind speed changed in range 6-45 m/s

(b) Rotor speed: the reference (green), the actual (red), and the estimated (blue)

Figure 11. The stable response at the constant rotor speed reference of 230 rad/s and the wind speed changed in range 6-45 m/s

Figure 12 showed that there was a narrow gap of the generated power between the optimal condition and the operation using the minimum critical reference for the rotor speed reference in the low speed range of wind (see zone A). But, in the medium and high speed ranges of wind, there was a wide gap of the generated power between the critical condition and the operation using the minimum critical reference for the rotor speed reference (see gap B in Figure 12). The wide gap showed that there was a challenge to generate power higher than the generated power using the constant rotor speed reference in the medium and high speed ranges of wind. The higher power would be generated by the controlling rotor speed in triangle area C in Figure 13.

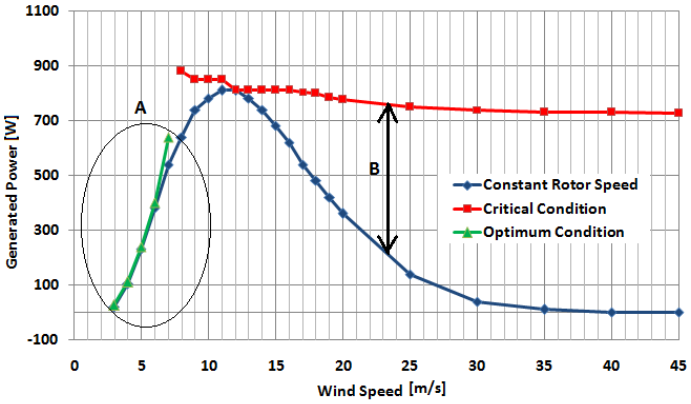

Figure 12. Generated power comparison

Another solution was suggested that the rotor speed in triangle area C in Figure 13 was controlled by setting the tip speed ratio. There was a wide gap of the tip speed ratio between the critical condition and the operation using the minimum critical reference for the rotor speed reference (see Figure 14). The gap of the tip speed ratio was wider than the gap of the capacity factor (see Figure 15). It showed that the controlling tip speed ratio had a bigger opportunity. To control the tip speed ratio, the wind turbine system had to be equipped with the wind speed sensor of anemometer.

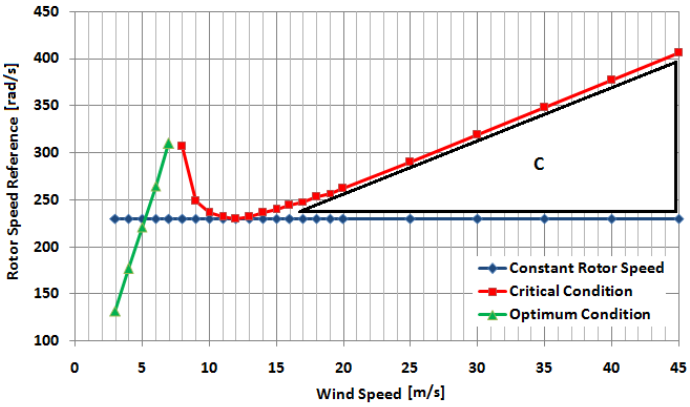

Figure 13. Rotor speed reference comparison

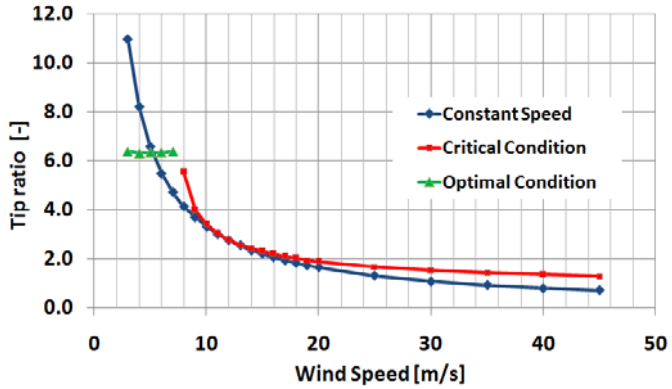

Figure 14. Tip speed ratio comparison

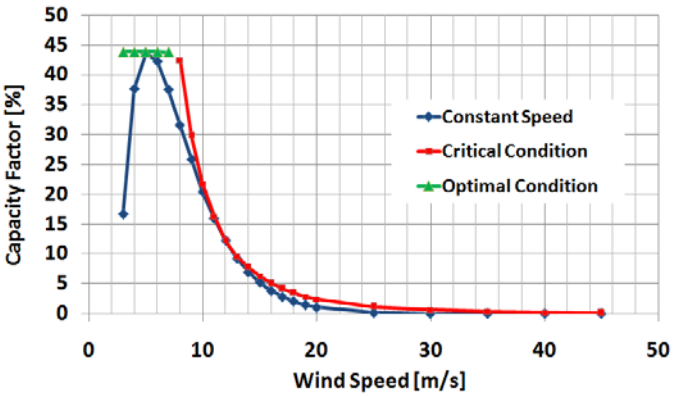

Figure 15. Capacity factor comparison

4. CONCLUSION

In the medium and high speed range of wind, there was a critical condition of the sensorless induction generator using flux weakening in the wind turbine application. The critical condition would happen when the rotor speed reached the critical rotor speed reference. The critical rotor speed reference was the highest of the rotor speed reference that still caused the stable response. The unstable condition was caused by the induction generator that received a power higher than its capacity, so its rotor speed couldn't be maintained at reference value. The first solution was suggested that the stable condition would be made by

setting the rotor speed reference at the minimum critical reference. The second solution was suggested that the controlling rotor speed in triangle area between the critical condition and the operation by using the minimum critical reference for the rotor speed reference. In the triangle area, the rotor speed was controlled by setting the tip speed ratio.

ACKNOWLEDGEMENTS

This research was supported by Ministry of Research, Technology and Higher Education, Republic of Indonesia and University of Indonesia (0563/UN2.R12/HKP.05.00/2015).

REFERENCES

[1] Feri Yusivar, Ridwan Gunawan, Harry Sudibyo S., Aries Subiantoro, Arnol Sinaga. *Over-speed Operation of Wind Turbine Induction Generator Using Field Weakening Control under Speed Sensorless Condition*. The 2nd International Conference on Nano Electronics Research and Education. Hamamatsu. 2014; 70-74.

[2] K. Viswanadha S. Murthy, M. Kirankumar, G.R.K. Murthy. A Performance Comparison of DFIG using Power Transfer Matrix and Direct Power Control Techniques. *International Journal of Power Electronics and Drive System*. 2014; 5(2): 176-184.

[3] A Kavitha, AV Suresh. A Novel Inter Connection of DFIG withGrid in Separate Excitation SMES System with Fuzzy Logic Control. *Bulletin of Electrical Engineering and Informatics*. 2015; 4(1): 43-52.

[4] Muldi Yuhendri, Mochamad Ashari, Mauridhi Hery Purnomo. Maximum Output Power Tracking of Wind Turbine using Intelligent Control. *TELKOMNIKA*. 2011; 9(2): 217-226.

[5] Ibrahim M. Alsofyani, Tole Sutikno, Yahya A. Alamri, Nik Rumzi Nik Idris, Norjulia Mohamad Nordin, Aree Wangsupphaphol. Experimental Evaluation of Torque Performance of Voltage and Current Models using Measured Torque for Induction Motor Drives. *International Journal of Power Electronics and Drive System*. 2015; 5(3): 433-440.

[6] K. Ramesh, Ch. Ravi Kumar, P. Bala Murali. Modeling and Implementation of Vector Control for Induction Motor Drive. *International Journal of Engineering Research and General Science*. 2015; 3(2): 80-91.

[7] Ridwan Gunawan, Feri Yusivar, Zuhal A. Kadir. *Field Oriented Control of An Induction Motor Speed Sensorless with Current Vector Controller, direct-quadrature Current Compensator and Full Order Observer In direct-quadrature Axis*. The 2nd Indonesian Japan Joint Scientific Symposium. Jakarta. 2006.

[8] F. Yusivar, S. Wakao. *Minimum Requirements of Motor Vector Control Modeling and Simulation Utilazing C MEX S-Function in Matlab/Simulink*. The 4th IEEE International Conference on Power Electronics and Drive Systems. Bali. 2001; 1: 315-321.

[9] A. Ben Ali, A. Khedher, M.F. Mimouni, R. Dhifaoui. Torque Maximization and Sensorless Control of Induction Motor in a Flux Weakening Region. *International Journal of Sciences and Techniques of Automatic Control & Computer Engineering IJ-STA*. 2009; 3(1): 972-985.

[10] Yusivar F, Wakao S. Field-*Weakening Scheme Combined with Saturated Voltage Control Strategy*. Proceedings of the IASTED International Conference on Modelling, Identification and Control. Grindelwald, Switzerland. 2004; 23: 412-146.

[11] T. Raghu, J. Srinivas Rao, S. Chandra Sekhar. Simulation of Sensorless Speed Control of Induction Motor Using APFO Technique. *International Journal of Computer and Electrical Engineering.* 2012; 4(4).

[12] Feri Yusivar, Kenji Uchida, Hiroyuki Haratsu, Shinji Wakao, Takashi Onuki. *Speed Adaptive Observer for Sensorless IM Drive using Combined Reference Frames*. Fifteenth Annual IEEE Applied Power Electronics Conference and Exposition (APEC). 2000; 1: 127-132.

[13] F. Yusivar, H. Haratsu, T. Kihara, S. Wakao, T. Onuki. *Performance comparison of the controller configurations for the sensorless IM drive using the modified speed adaptive observer*. 8th International Conference on Power Electronics and Variable Speed Drives. 2000; 495: 194-200.

BIOGRAPHIES OF AUTHORS

Nanda Avianto Wicaksono was born in Jakarta, Indonesia. He received his bachelor and master degrees in Electrical Engineering at Institute Technology of Bandung, Indonesia in 1998 and 2002. He is currently the student in Electrical Engineering at University of Indonesia and the researcher in Research and Development Agency, Ministry of Energy and Mineral Resources, Republic of Indonesia. His research interests are in control system, electrical drive, power electronics, and renewable energy.

Abdul Halim was born in Jakarta, Indonesia He received his bachelor and master degree in Electrical Engineering at Keio University, Japan in 1995 and 1997, and also completed his Doctor degree in 2000 at Tokyo Institute of Technology, Japan. He is currently the lecturer in Electrical Engineering at University of Indonesia. His research interests are in control system engineering, power system engineering, computer simulation, intelligent engineering, and applied mathematics.

Aries Subiantoro was born in Jakarta, Indonesia. He received his Bachelor degree in Electrical Engineering at University of Indonesia in 1995, and completed his Doctor degree in 2013 at University of Indonesia. His research interests are in model and simulation, intelligent control system, and model predictive control system.

Feri Yusivar was born in Bandung, Indonesia. He received his bachelor degree in Electrical Engineering at University of Indonesia in 1992, and completed his Doctor degree in 2003 at Waseda University, Japan. He is currently the Head of Control Laboratory in Electrical Engineering at University of Indonesia. His research interests are in control system, electrical drive, power electronics, and renewable energy.